Interaction of antimicrobial peptide protegrin with biomembranes

David Gidalevitz*†, Yuji Ishitsuka†‡, Adrian S. Muresan§, Oleg Konovalov¶, Alan J. Waring‖**, Robert I. Lehrer‖, and Ka Yee C. Lee‡††

*Department of Chemical Engineering, University of Leeds, Leeds LS2 9JT, United Kingdom; Departments of ‡Chemistry and §Physics, Institute for Biophysical Dynamics and the James Franck Institute, University of Chicago, Chicago, IL 60637; ¶European Synchrotron Radiation Facility, B.P. 220, 38043 Grenoble Cedex 9, France; ‖Department of Medicine, University of California, Los Angeles, CA 90095; and **Department of Pediatrics, University of California School of Medicine, Harbor-University of California Los Angeles Medical Center, Torrance, CA 90502

Edited by William F. DeGrado, University of Pennsylvania School of Medicine, Philadelphia, PA, and approved March 5, 2003 (received for review August 6, 2002)

The antimicrobial peptide protegrin-1 (PG-1) interacts with membranes in a manner that strongly depends on membrane lipid composition. In this research we use an approach representing the outer layers of bacterial and red blood cell membranes with lipid monolayers and using a combination of insertion assay, epifluorescence microscopy, and surface x-ray scattering to gain a better understanding of antimicrobial peptide's mechanism of action. We find that PG-1 inserts readily into anionic dipalmitoyl-phosphatidylglycerol, palmitoyl-oleoyl-phosphatidylglycerol, and lipid A films, but significantly less so into zwitterionic dipalmitoyl-phosphatidylcholine, palmitoyl-oleoyl-phosphatidylcholine, and dipalmitoyl-phosphatidylethanolamine monolayers under similar experimental conditions. Epifluorescence microscopy shows that the insertion of PG-1 into the lipid layer results in the disordering of lipid packing; this disordering effect is corroborated by grazing incidence x-ray diffraction data. X-ray reflectivity measurements further point to the location of the peptide in the lipid matrix. In a pathologically relevant example we show that PG-1 completely destabilizes monolayer composed of lipid A, the major component in the outer membrane of Gram-negative bacteria, which is likely to be the mechanism by which PG-1 disrupts the outer membrane, thus allowing it to reach the target inner membrane.

Antimicrobial peptides secretion is a part of a natural immune response of many living organisms. These peptides mount a rapid response to infection by diverse bacterial species. For many antimicrobial peptides, it appears that the main target is the lipid bilayer itself, rather than some specific protein receptor(s) within the cell membrane (1–3). Since D-enantiomers of antimicrobial peptides frequently exhibit similar activity to their L-counterparts (4–6), they evidently interact with achiral components of the cell membrane.

Despite the growing interest in these peptides, the molecular mechanism involved in antimicrobial peptide-mediated rupturing events of pathogenic cell membranes still remains unclear. Three models of membrane rupturing mechanisms have been proposed to date: barrel-stave, carpet, and toroidal. According to the barrel-stave model (7–11), peptides bound to membrane recognize each other and oligomerize, and the oligomer inserts into the hydrophobic core of the membrane, forming a transmembrane pore. Upon oligomerization, antimicrobial peptides orient themselves, allowing the hydrophobic surface to interact with the hydrophobic core of the membrane and the hydrophilic surface to point inward to create a hydrophilic pore. The carpet model (12–14) suggests that antimicrobial peptides initially bind to and cover the surface of the target membrane. The electrostatic interaction between the peptide and the lipid head group imposes strain in the membrane, and membrane permeation is induced only at sites where local peptide concentration is higher than certain threshold values. In the toroidal model (15–17), peptides similarly bind and interact with lipid head groups, imposing a positive curvature strain on membranes (e.g., magainin 2) and producing channels where the polar headgroup region expands to form "toroidal" pores. The activity of these antimicrobial peptides is not always caused merely by the breakdown of the permeability barrier in microbes (14, 18). Other membrane-dependent processes, such as translocation of cytotoxic peptides across the membrane to the cytoplasm and facilitation of transbilayer lipid diffusion (which leads to the loss of lipid asymmetry in the membrane), may also be involved in the action of some of these peptides (19).

An intriguing feature of these peptides is their ability to distinguish prokaryotic from eukaryotic cells. The lipid composition on the surface of a prokaryotic cell is rather different from that of an eukaryotic cell (20). The outer leaflet of mammalian cell membranes mainly comprises phosphatidylcholine (PC), sphingomyelin, and cholesterol, which are charge neutral at physiological pH. In contrast, bacterial membranes include substantial amounts of negatively charged phospholipids, such as phosphatidylglycerol and cardiolipin (21). In Gram-negative bacteria, the outer leaflet of their outer membrane bilayer consists mostly of lipopolysaccharide, a polyanionic molecule.

To elucidate the mechanism by which antimicrobial peptides carry out their activity, it is crucial to obtain a better understanding of the interaction between them and the lipids found in cell membranes. Fig. 1 is an electron micrograph of *Escherichia coli* cells exposed to a β-sheet antimicrobial peptide, protegrin-1 (PG-1). The outer membrane is greatly expanded and thrown into numerous folds (microvilli) that are absent in untreated controls. This work examines the interaction between PG-1 and a series of model lipid monolayers used to simulate the outer leaflet of cell membranes. To monitor the level of insertion of PG-1 into these monolayers, we have carried out Langmuir trough experiments and recorded relative changes in surface area of monolayers held at constant surface pressure after the introduction of PG-1 into the subphase. We have also assessed the subsequent effects on the film's surface morphology with epifluorescence microscopy. Our results indicate that PG-1 molecules insert into membranes at a significantly higher degree if they are composed of negatively charged phospholipids, rather than zwitterionic lipids. We have observed drastic destabilization effects on lipid A monolayers, which point to a possible mechanism by which the peptide is able to penetrate to the inner membrane to carry out its lytic activity on Gram-negative bacteria. Grazing incidence x-ray diffraction (GIXD) data clearly shows that the presence of PG-1 disrupts lipid ordering, whereas x-ray reflectivity (XR) measurements carried out on a negatively charged dipalmitoyl-phosphatidylglycerol (DPPG) film after peptide inser-

This paper was submitted directly (Track II) to the PNAS office.

Abbreviations: PC, phosphatidylcholine; DPPC, dipalmitoyl-PC; POPC, palmitoyl-oleoyl-PC; PG-1, protegrin-1; DPPG, dipalmitoyl-phosphatidylglycerol; PE, phosphatidylethanolamine; DPPE, dipalmitoyl-PE; POPG, palmitoyl-oleoyl-phosphatidylglycerol; XR, x-ray reflectivity; GIXD, grazing incidence x-ray diffraction.

†D.G. and Y.I. contributed equally to this work.

††To whom correspondence should be addressed. E-mail: kayeelee@uchicago.edu

 www.pnas.org/cgi/doi/10.1073/pnas.0934731100

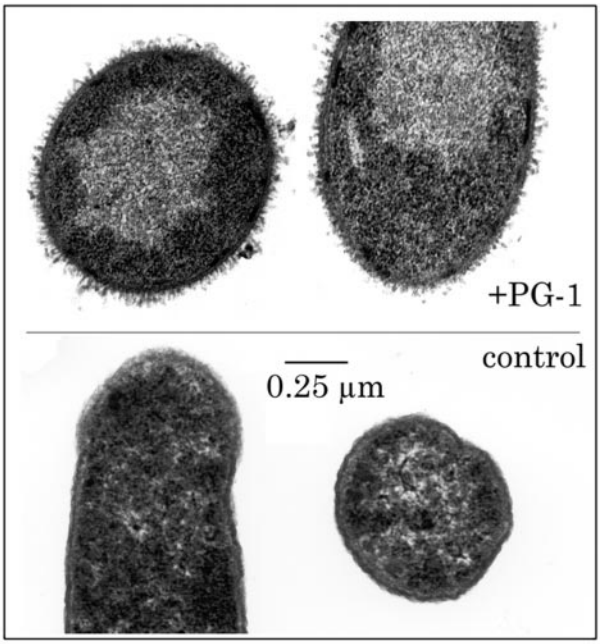

Fig. 1. Effects of PG-1 on *E. coli* morphology. (*Upper*) Bacteria were exposed to 50 μg/ml PG-1 for 15 min. (*Lower*) Bacteria are untreated controls. The outer membrane of the treated organisms is greatly expanded and displays innumerable microvilli.

tion further allow us to obtain molecular-level information on how the protegrin peptide associates with the lipid film.

PG-1 is an 18-aa, amidated peptide (NH_2-RGGRLCYCRRRFCVCVGR-$CONH_2$) originally isolated from porcine leukocytes (22). Protegrins are part of the porcine immune system and appear to be functionally analogous to defensins in humans (23) and circular (theta) defensins in the rhesus monkey (24). NMR studies showed that PG-1 adopts a one-turn β-hairpin structure that includes two disulfide bonds (25, 26).

In vitro, PG-1 is known to be toxic for many bacteria including *E. coli* (22), *Listeria monocytogenes* (22, 27), and *Neisseria gonorrhoeae* (28, 29). It also kills the fungus *Candida albicans* (22, 30) and can protect cells from *in vitro* HIV infection (31). PG-1 has been found to cause ionic leakage or channel formation in planar lipid bilayers (32). Moreover, channel formation is favored at a negative transmembrane voltage, which mimics the membrane potential of a microbial target cell. Experiments show that channel activity and conductance are enhanced by the presence of lipopolysaccharide, suggesting that Gram-negative bacterial outer membranes may be especially sensitive to PG-1 action (32).

Interestingly, PG-1 reacts with erythrocytes from some eukaryotes, but not others. Recent studies have indicated that PG-1 shows hemolytic activity toward human erythrocytes (33), but not against red blood cells from goat or sheep. The differences may result from the different lipid compositions of these cells. Phosphatidylethanolamine (PE), for example, accounts for 33.3% of human erythrocyte membrane mass, but composes 47.3% and 67.8% of goat and sheep erythrocytes, respectively (34). Moreover, PC is absent in goat and sheep erythrocyte membranes, but makes up 30.3% of the lipid composition in humans (34, 35). Can these variations in membrane lipid composition account for the difference in PG-1 activity observed in the various red blood cells?

Various lipid systems have been examined in this study. To address the question on red blood cell selectivity, we have examined the interactions of PG-1 with zwitterionic dipalmitoyl-PE (DPPE) and dipalmitoyl-PC (DPPC). Since the outer layers of bacterial membranes are predominantly negatively charged, and in most cases contain substantial amounts of phosphatidylglycerol, we have chosen DPPG as a model lipid system for bacterial membranes. Although these saturated phospholipids are excellent model systems to address the effect of headgroup charge on PG-1 insertion, biological membranes comprise a significant amount of unsaturated lipids. Therefore, we have also examined the interaction between PG-1 and unsaturated lipids such as palmitoyl-oleoyl-PC (POPC) and palmitoyl-oleoyl-phosphatidylglycerol (POPG). As the outer leaflet of the outer membrane of Gram-negative bacteria contains lipopolysaccharide, whose lipid anchoring portion, lipid A, is a complex molecule consisting primarily of fatty acids and phosphate groups bonded to a carbohydrate backbone, lipid A was used to model the action of PG-1 on Gram-negative bacteria.

Materials and Methods

Langmuir Trough and Epifluorescence Experiments. All surface pressure-area isotherms were collected by using a Teflon Langmuir trough equipped with a Wilhelmy plate. The home-built Teflon Langmuir trough (27.5 cm $\times$ 6.25 cm $\times$ 0.63 cm) equipped with two identical mobile Teflon barriers (l = 6.25 cm) enables compression or expansion of monolayers spread at the air-water interface, thereby increasing or reducing the surface pressure (defined as the difference in surface tension between a pure interface and one with a monolayer), respectively. Dulbecco's PBS without calcium and magnesium was used as the subphase. The subphase temperature was maintained at 30°C $\pm$ 0.5°C through the use of a homebuilt control station comprised of thermoelectric units joined to a heat sink held at 20°C by a Neslab Instruments (Portsmouth, NH) RTE-100 water circulator. A resistively heated indium tin oxide-coated glass plate was placed over the trough to minimize dust contamination, air currents, and evaporative losses and to prevent condensation of water on the microscope objective.

The Langmuir trough is positioned on translation stages that permit scanning along the air-water interface in the x, y, and z directions. This assembly is fixed to a custom-built microscope stage for simultaneous epifluorescence microscopy with a $\times$50 long working distance objective lens. Excitation between 530 and 590 nm and emission between 610 and 690 nm was gathered through the use of a HYQ Texas red filter cube; 0.5 mol% of lipid-linked Texas-red (TR-DHPE) dye from Molecular Probes was incorporated into the spreading phospholipid solutions. Because of steric hindrance, the dye partitions into the disordered phase, rendering it bright and the ordered phase dark. Images from the fluorescence microscope were collected at a video rate of 30 frames per s by using a silicon intensified target camera and recorded on SuperVHS-formatted videotape with a recorder. This assembly permits the monolayer morphology to be observed over a large lateral area while isotherm data are obtained concurrently. The entire apparatus is set on a vibration isolation table.

DPPE, DPPC, DPPG, POPC, and POPG were purchased from Avanti Polar Lipids, and lipid A (diphosphoryl, from *E. coli* F583) was purchased from Sigma-Aldrich. All lipids were used without further purification. The synthesis of PG-1 has been described (26). Monolayers of DPPE, DPPC, DPPG, POPC, and POPG phospholipids were deposited quantitatively from chloroform (Fisher Spectranalyzed) solution, whereas lipid A was deposited from 74:23:3 chloroform/methanol/water solution. To determine under what lipid packing conditions PG-1 would insert into model lipid systems, the monolayer was compressed to a predetermined pressure by two symmetrical barriers. The pressure was maintained to within $\pm$0.2 mN/m throughout the experiment with a built-in feedback system. PG-1 was dissolved in 0.01% acetic acid to a concentration of 1 mg/ml. To examine the interaction between the peptide and the lipid monolayer, an aliquot of the PG-1 solution was injected into the buffer subphase, resulting in a final PG-1 concentration of 0.025 mg/ml. This peptide concentration was used to match with condi-

tions used in examining lytic activities PG-1 in live cells. The relative change in area per molecule, $\Delta A/A$, was monitored during and after the introduction of the peptide into the subphase. With the surface pressure held constant, any increase in $\Delta A/A$ after injection indicates insertion of the peptide into the phospholipid monolayer because the peptide is taking up space at the interface. The level of peptide insertion therefore correlates with the level of increase in $\Delta A/A$.

X-Ray Scattering Experiments. XR experiments were carried out at beamline X19C of the National Synchrotron Light Source, Brookhaven National Laboratory, Upton, NY, using a custom-built liquid surface diffractometer (36) with incident wavelength of $\lambda = 1.54$ Å. A sealed and thermostated Langmuir trough equipped with a Wilhelmy balance was supported on a vibration isolation stage on the diffractometer. Compression of the monolayer was achieved by moving a motorized Teflon ribbon. Both the trough and the ribbon assembly were enclosed in temperature-controlled aluminum housing with a Kapton window.

The monochromatic x-ray beam was deflected toward the water surface via Bragg reflection from a Si(111) crystal. The x-rays were collimated with a set of four-jaw slits. These slits were always set to optimize the resolution in the scattering plane while increasing the signal by lowering the resolution out of the scattering plane. A beam monitor before the sample provided data for the normalization of the incident beam intensity. The reflected beam intensity was measured with a NaI scintillation detector as a function of incident angle. Calibrated attenuators between the sample and the detector were inserted and removed as necessary during the course of the XR scan to use only the linear regime of the detector.

GIXD experiments were carried out at the ID 10B Tröika II beamline at European Synchrotron Radiation Facility, Grenoble, France (37). The Langmuir trough was equipped with a moveable single barrier, and the surface pressure was measured with a Wilhelmy balance. The vessel containing the trough was sealed and filled with a flow of water-saturated helium to reduce evaporation of the subphase and parasitic scattering from the air.

To perform GIXD measurements the downstream mirror was used to set the angle of incidence α_i onto the air/water interface at $\alpha_i = 0.85\ \alpha_c$, where α_c is the critical angle for total external reflection. The diffracted beam was detected by a linear position-sensitive detector (PSD) that records an intensity profile as a function of the vertical scattering angle. A Soller collimator in front of the PSD provided a horizontal resolution of $\Delta Q_{xy} = 0.006$ Å^{-1}.

Results

Peptide Insertion Measurements. Insertion studies were first performed on DPPE, DPPC, and DPPG monolayers; isotherms of pure DPPE, DPPC, and DPPG are shown in Fig. 2. Insertion behavior at various constant pressures has been examined. Here, we present results obtained at 20 mN/m before and after introducing PG-1. Different levels of insertion of the peptide into the lipid layer were found, with DPPE being the least affected by PG-1 and DPPG the most affected. With DPPE monolayers, the area per molecule changed only by 11% after injection of PG-1 into the subphase (Fig. 3, solid line). With DPPC films, the area per molecule increased by 59% (Fig. 3, dashed line). PG-1 inserted much more extensively into DPPG monolayers, increasing the relative area per lipid molecule by 121% (Fig. 3, dotted line). Unlike bacteria, outer leaflets of red blood cell membranes do not contain significant amounts of anionic phospholipids. Consequently, the very low level of PG-1 interaction with DPPE monolayers, the substantially lower level of PE in human erythrocytes, and the absence of PC in sheep and goat may explain why the peptide lyses human red blood cells, but not these of sheep and goat (34). Since all three lipids bore identical acyl chains, yet showed different insertion affinities for PG-1, we concluded that phospholipid headgroups were crucial sites for initial interactions with PG-1.

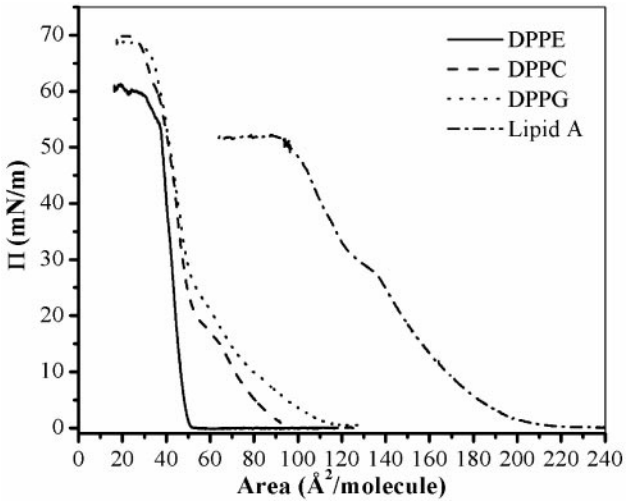

Fig. 2. Surface pressure–area isotherms for DPPE, DPPC, DPPG, and lipid A on buffered saline at 30°C.

An estimate of the PG-1/lipid ratio at the interface can be deduced from these experiments, given the initial and final areas, as well as the previously determined dimensions of the peptide from NMR data (≈8 Å in diameter and 30 Å in length) (26). In the case of DPPG, if we assume similar area occupied by each lipid molecule before and after PG-1 insertion, the PG-1/DPPG ratio is found to be 1:3 at 20 mN/m under constant pressure conditions. Similar insertion assays can be carried out by first compressing the film to 20 mN/m, followed by injection of PG-1 into the subphase under constant area conditions, with subsequent PG-1 insertion resulting in a pressure increase under constant area conditions. A much reduced PG-1/DPPG ratio of 1:17 is found if the long axis of the peptide is assumed to be perpendicular to the interface, and a ratio of 1:20 if parallel. Given the same initial surface pressure, it should not be surprising that the level of peptide incorporation is larger for constant pressure experiments with the packing density remaining constant throughout the experiment. In contrast, the surface pres-

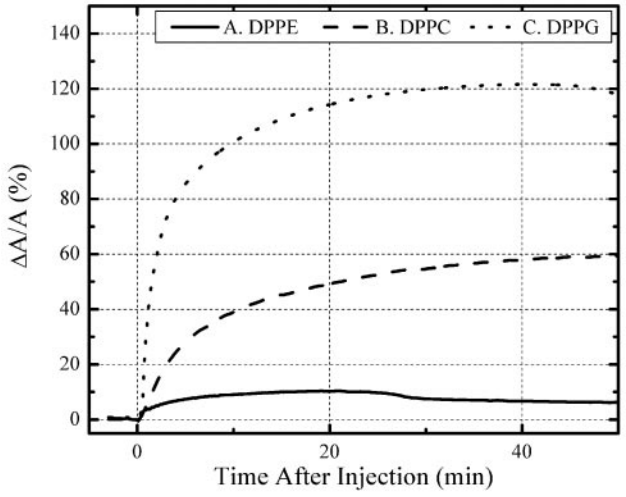

Fig. 3. Percentage change of area after injection of PG-1 into aqueous subphase at 20 mN/m. Solid line, very small insertion into DPPE monolayer (11%). Dashed line, more pronounced insertion (59%) into DPPC. Dotted line, substantial insertion into DPPG (121%).

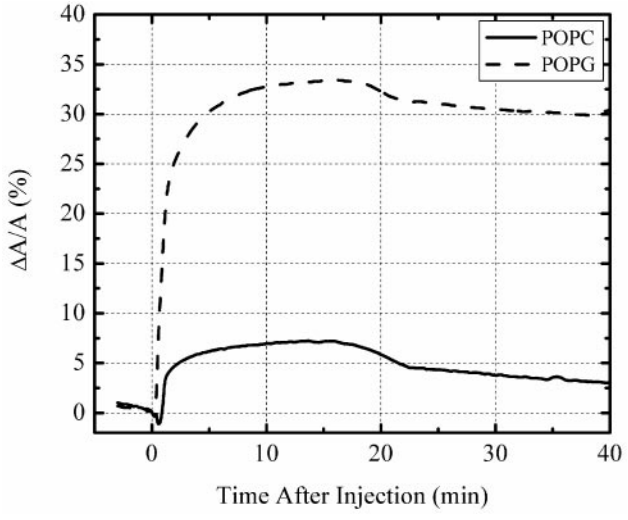

Fig. 4. Percentage change of area after injection of PG-1 into aqueous subphase at 30 mN/m. Very small insertion was observed in a POPC monolayer (7%), but much more pronounced insertion (33%) was found in a POPG film.

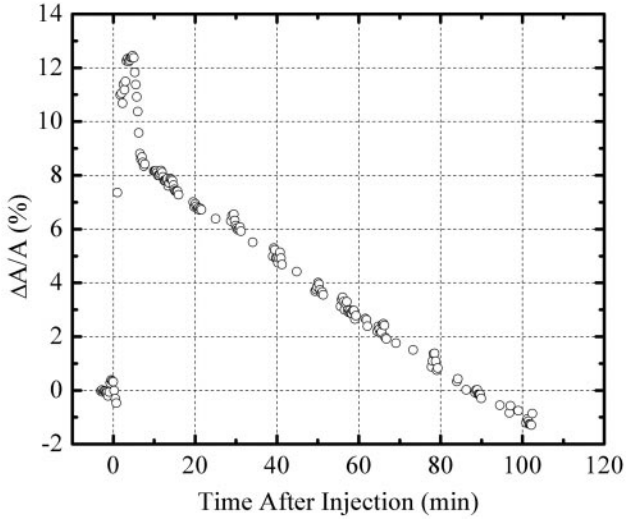

Fig. 5. Insertion of PG-1 peptide into lipid A monolayer at constant surface pressure of 35 mN/m. Rapid insertion for the first 5 min (12%) after injection, and then gradual collapse of lipid A monolayer where the area per lipid molecule decreased to values below its initial value.

sure increases upon peptide insertion in the constant area case, resulting in a more tightly packed film and hindering subsequent peptide incorporation into the monolayer.

To better mimic biological membranes, we carried out insertion studies using lipids with unsaturated tails to enhance the fluidity in the system. Fig. 4 shows the insertion profiles of PG-1 into POPC and POPG monolayers at 30 mN/m. Similar to their saturated counterparts, PG-1 inserts much more readily into phosphatidylglycerol versus PC monolayers. Although PG-1 barely inserts into DPPC at this pressure (data not shown), it is capable of inserting into POPC monolayers to a small extent (7%) and into POPG film to a large extent (33%). This finding clearly demonstrates that the increased fluidity of the film afforded by the unsaturated tails significantly eases PG-1 insertion.

A completely different insertion profile has been observed with lipid A monolayers. The isotherm of pure lipid A is shown in Fig. 2. Upon injection of PG-1 into the subphase underneath a lipid A monolayer at a surface pressure of 20 mN/m, the area per molecule increased by 117% (data not shown), which is comparable to PG-1 insertion level to another negatively charged lipid, DPPG (121%). Although protegrin does not insert into DPPC or DPPG monolayers at 35 mN/m, PG-1 penetrates readily into lipid A monolayers at this pressure and has a profound effect on the film stability (Fig. 5). In the first 5 min after introduction of PG-1 into the subphase, the area increases by 12%, then gradually decreases to below the original value before PG-1 injection. One possible explanation for this phenomenon is that there exists a threshold concentration for PG-1 insertion, beyond which results in destabilization of the lipid A film. The ability of PG-1 to destabilize the lipid A monolayer points to a possible mechanism by which PG-1 permeabilizes the outer membrane of Gram-negative bacteria, thus getting access to the inner membrane that constitutes the real target for lytic activities.

Epifluorescence Microscopy Measurements. The surface morphology of these insertion events was monitored by using epifluorescence microscopy. DPPE monolayers at 20 mN/m show a slight change in their surface morphology after PG-1 injection, displaying a small increase in the bright disordered phase between dark domains of ordered condensed phase (Fig. 6 *A* and *B*). This finding indicates a small degree of interaction between PG-1 and the PE monolayer. In contrast, DPPC monolayer insertion results at 20 mN/m (Fig. 6 *C* and *D*) show a significant change in the lipid layer morphology after peptide insertion. A substantial transformation of their dark (ordered) lipid domains into bright (disordered) ones is consequent to the ability of PG-1 to insert into the PC monolayer and disrupt phospholipid ordering. Peptide-induced morphological changes are prominent in DPPG monolayers as well (Fig. 6 *E* and *F*). DPPG monolayers showed arrays of dark branched condensed (ordered) domains separated by bright "fluid" (disordered) phase (Fig. 6*E*). Immediately after injecting PG-1, the bright areas increased progressively, and by 30 min (Fig. 6*F*), condensed-phase domains greatly decreased in size, with the majority of the film in a peptide-rich fluid phase. Epifluorescence measurements on POPC, POPG, and lipid A at the same pressure did not show any phase separation because its unsaturated hydrocarbon chains could not pack densely and remained disordered at this surface pressure and temperature.

X-Ray Measurements. To examine the effect of PG-1 insertion on lipid packing and to assess the location of the peptide in the liquid matrix, we carried out x-ray scattering studies at room temperature on the DPPG/PG-1 system that has shown the largest extent of peptide insertion. Before PG-1 injection DPPG was compressed to $\Pi = 20$ mN/m and kept at a constant area. GIXD and XR measurements were performed on a pure DPPG monolayer before PG-1 insertion and after the system has equilibrated after protegrin injection.

The GIXD data for the DPPG film at 20 mN/m before and after the injection of PG-1 are shown in Fig. 7 as solid and dotted lines, respectively. Pure DPPG data yield two Bragg peaks from the condensed phase at $Q_{xy} = 1.36$ Å^{-1} and $Q_{xy} = 1.46$ Å^{-1}, corresponding to d-spacings of 4.62 and 4.30 Å, respectively. This result translates to a centered orthogonal unit cell with unit cell dimensions $a = 5.48$ Å and $b = 8.60$ Å and an area of 47.1 Å^2 per DPPG molecule. Analysis of the Bragg rod profile gives a molecular tilt of 33° for the lipid molecules in the condensed phase that give rise to these scattered peaks. As clearly shown in Fig. 7, introduction of PG-1 resulted in the complete disappearance of the Bragg peaks (dotted line in Fig. 7). This finding points to the disordering of the lipid packing upon PG-1 insertion and corroborates our epifluorescence microscopy results of the

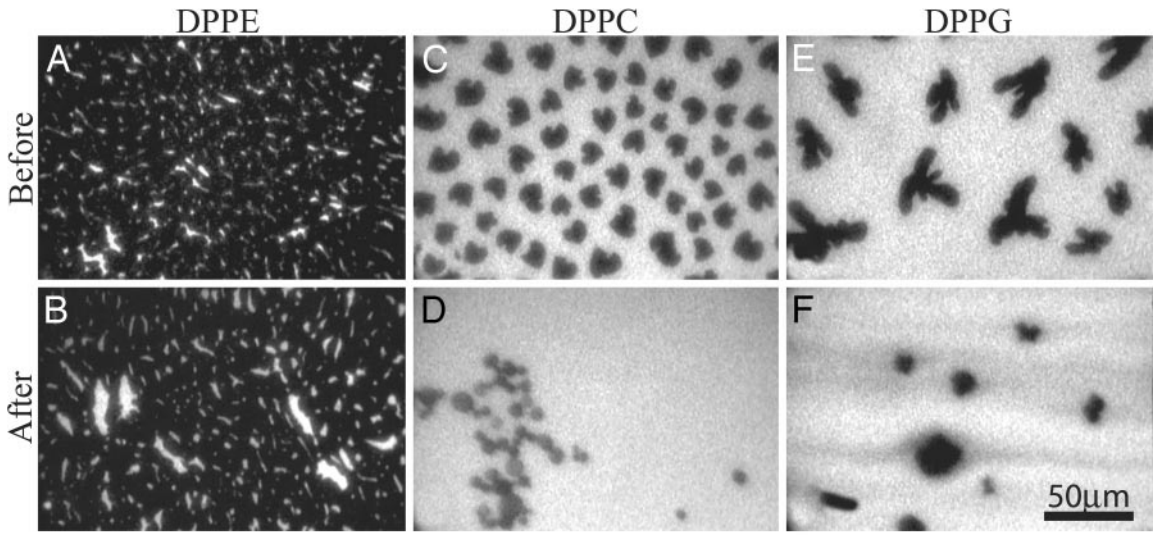

Fig. 6. Epifluorescence micrographs showing the phospholipid films before (*A*, *C*, and *E*) and after (*B*, *D*, and *F*) injecting PG-1 at 20 mN/m. (*A* and *B*) DPPE. (*C* and *D*) DPPC. (*E* and *F*) DPPG. The relative increase in bright area from *A* to *B*, *C* to *D*, and *E* to *F* corresponds to the increase in the disordered fluid phase caused by PG-1 insertion. Images *B*, *D*, and *F* were taken after the maximum lipid area per molecule change was reached and no further morphological changes were observed.

reduction in area fraction of the dark condensed-phase domains conducted at 30°C (Fig. 6 *E* and *F*). Decreases in Bragg peak intensities in DPPC and DPPE monolayers after PG-1 injection have also been observed. Unlike for the DPPG case, the peaks for DPPC and DPPE do not completely disappear: those of DPPC suffer a large degree of intensity loss, whereas that of DPPE decreases only by a small amount. These results agree well with the extent of insertion observed in constant pressure and epifluorescence microscopy measurements conducted at 30°C. It should be pointed out that the intensity of the Bragg peak can have a small variation from scan to scan because of possible inhomogeneity in domain distribution on the monolayers.

XR is determined by the Fourier transform of the gradient of the electron density perpendicular to the liquid surface, and thus yields monolayer's electron density profile perpendicular to the interface (38). Analysis of the reflectivity data were performed by modeling the interface as a stack of slabs with different electron densities, ρ_i/ρ_s, and thicknesses, L_i, and applying a least-squares fit to the experimental data. Here i identifies the slab, with t signifying the tail region, h the headgroup region, and p the pure peptide adsorption region when referring to different slabs in the paragraph that follows. ρ_s is the subphase electron density.

The XR data for pure DPPG film (Fig. 8, squares) were best fitted with a two-slab model yielding a hydrocarbon tail density (ρ_t/ρ_s) of 0.92 and a hydrocarbon tail slab thickness (L_t) of 12.3 Å, as well as a headgroup electron density (ρ_h/ρ_s) of 1.30 and headgroup slab thickness (L_h) of 8.4 Å (Fig. 8, solid line). The reflectivity profile changed dramatically after PG-1 was introduced (Fig. 8, circles). Extensive fitting of the data indicates that they can no longer be adequately represented by a two-slab model, but good agreement can be achieved with a three-slab model (Fig. 8, dashed line). The first slab (ρ_t/ρ_s = 1.22 and L_t = 13.9 Å) corresponds to the lipid tail region, whereas the second

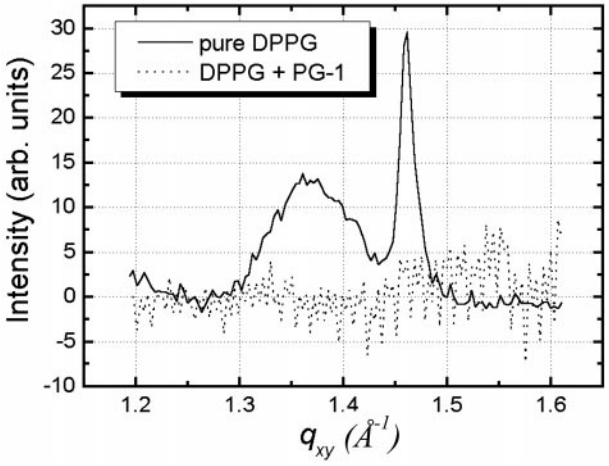

Fig. 7. Bragg peaks from GIXD measurements on a DPPG monolayer before (solid line) and after (dotted line) PG-1 injection into the subphase. The initial Bragg peaks from scattering of ordered structure in the monolayer vanish upon PG-1 insertion.

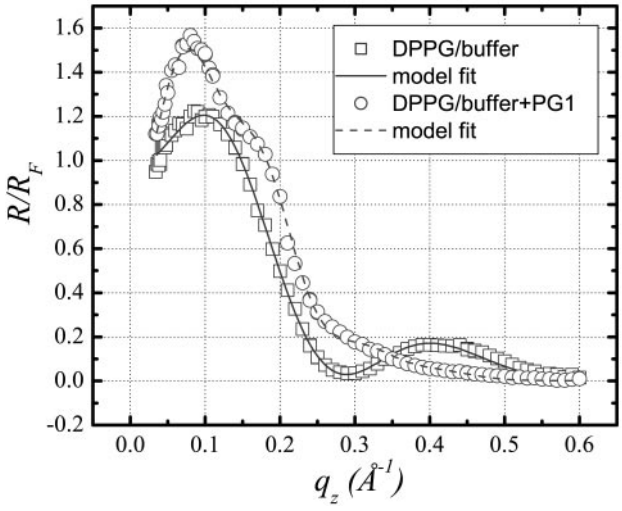

Fig. 8. XR data and corresponding fit for DPPG taken at 20 mN/m before and after PG-1 equilibrated after its injection underneath the monolayer.

slab (ρ_h/ρ_s = 1.27, L_h = 7.0 Å) corresponds to the headgroup region of the DPPG monolayer. As PG-1 has an electron density larger than that of the hydrocarbon tail region but smaller than that of the headgroup region, the decreased electron density of the headgroup region and the increased density of the aliphatic tail area upon PG-1 injection are indicative of insertion of PG-1 into the DPPG film. Apart from the peptide insertion into the lipid monolayer indicated by the change in electron densities in the first two slabs, our analysis shows an additional third slab (ρ_p/ρ_s = 1.07, L_p = 27.2 Å) is needed to adequately fit the data. This additional slab most likely signifies the adsorption of PG-1 underneath the DPPG monolayer.

We conclude from the above that PG-1 both inserted into the DPPG membrane and adsorbed to its surface. The sum of the first two slabs gave a total thickness of $L_1 + L_2$ = 20.9 Å, equivalent to that of a pure DPPG monolayer (20.7 Å). Because of its two disulfide bonds, the central portion of PG-1 (residues 6–16) is relatively restricted in shape and the physical dimensions of a PG-1 molecule are ≈8 Å wide by 25 Å up to 35 Å long (26). Thus, the measured thickness (27 Å) of the additional third slab suggests that the peptide likely orients with its long axis perpendicular to the interface, just as the increased electron density of the tail region indicates at least partial insertion of some protegrin molecules.

Conclusions

Overall, our data suggest that the ability of PG-1 to bind and perturb monolayers of lipid A and phosphatidylglycerol equips it to preferentially damage the membranes of bacteria over those of eukaryotic cells. The degree of PG-1 insertion into anionic DPPG, POPG, or lipid A monolayers is significantly larger than that of zwitterionic DPPE, DPPC, and POPC. The disordering effect on lipid packing upon PG-1 insertion has been observed at 20 mN/m by epifluorescence microscopy and GIXD experiments, with the degree of disruption corresponding to the extent of PG-1 incorporation. Although PG-1 completely disrupts the structure of anionic DPPG, it significantly disorders the lipid structure of zwitterionic DPPC, but only affects that of zwitterionic DPPE marginally. The activity of PG-1 is therefore quite different from that of the α-helical antimicrobial frog skin peptide PGLa reported recently to disrupt only the structure of anionic monolayers, but not that of zwitterionic ones like DPPC (37). The small degree of protegrin interaction with DPPE and the nature of its interaction with DPPC may explain the targeting selectivity of PG-1 for DPPC-rich human erythrocytes over DPPE-rich, DPPC-deficient sheep and goat erythrocytes. The reflectivity data indicate that PG-1 both inserts into and adsorbs to the DPPG monolayer. Most intriguingly, insertion of PG-1 leads to the complete destabilization of lipid A films.

Bacterial membranes are important for maintaining microbial homeostasis, metabolism, and viability. The present studies suggest that the deleterious effects of PG-1 on Gram-negative bacterial membranes are dictated largely by the abundance of lipid A and anionic phospholipids in microbial outer and inner membranes. Just as the insertion of PG-1 into lipid A monolayers can explain its ability to expand and permeabilize the outer membrane of *E. coli*, similar effects on phosphatidylglycerol-rich monolayers could contribute to its ability to permeabilize the inner (cytoplasmic) membrane. This inherent ability to "recognize" and interact with structures or structural patterns that are intrinsic to microbes and absent in eukaryotic cells may augur well for the development of protegrins and other antimicrobial peptides as future therapeutic agents.

We are grateful to Stuart A. Rice for the beam time and Zhengqing Huang for his assistance with x-ray experiments at Brookhaven. We are also indebted to Karl Lohner and Stuart A. Rice for their useful comments. D.G. and Y.I. were supported by David and Lucile Packard Foundation Grant 99-1465. A.S.M. was supported by Alzheimer's Association Grant IIRG-9901175 and American Health Association Foundation Grant A-1999057. K.Y.C.L. is grateful for the support of the Henry and Camille Dreyfus Foundation (Grant NF-98-048) and the Alfred P. Sloan Foundation (Grant BR-4028). R.I.L. and A.J.W. were supported by National Institutes of Health Grants AI 22839 and AI 37945. The experimental apparatus was made possible by National Science Foundation Chemistry Research Instrumentation Facility/Junior Faculty Grant CHE-9816513.

1. Lohner, K. & Epand, R. M. (1997) *Adv. Biophys. Chem.* **6,** 53–66.
2. Lohner, K., Latal, A., Lehrer, R. I. & Ganz, T. (1997) *Biochemistry* **36,** 1525–1531.
3. Lohner, K. & Prenner, E. J. (1999) *Biochim. Biophys. Acta* **1462,** 141–156.
4. Wade, D., Boman, A., Wahlin, B., Drain, C. M., Andreu, D., Boman, H. G. & Merrifield, R. B. (1990) *Proc. Natl. Acad. Sci. USA* **87,** 4761–4765.
5. Bessalle, R., Kapitkovsky, A., Gorea, A., Shalit, I. & Fridkin, M. (1990) *FEBS Lett.* **274,** 151–155.
6. Blondelle, S. E., Takahashi, E., Dinh, K. T. & Houghten, R. A. (1995) *J. Appl. Bacteriol.* **78,** 39–46.
7. Juvvadi, P., Vunnam, S. & Merrifield, R. B. (1996) *J. Am. Chem. Soc.* **118,** 8989–8997.
8. Ehrenstein, G. & Lecar, H. (1977) *Q. Rev. Biophys.* **10,** 1–34.
9. Christensen, B., Fink, J., Merrifield, R. B. & Mauzerall, D. (1988) *Proc. Natl. Acad. Sci. USA* **85,** 5072–5076.
10. Matsuzaki, K., Harada, M., Handa, T., Funakoshi, S., Fujii, N., Yajima, H. & Miyajima, K. (1989) *Biochim. Biophys. Acta* **981,** 130–134.
11. He, K., Ludtke, S. J., Worcester, D. L. & Huang, H. W. (1996) *Biophys. J.* **70,** 2659–2666.
12. Pouny, Y., Rapaport, D., Mor, A., Nicolas, P. & Shai, Y. (1992) *Biochemistry* **31,** 12416–12423.
13. Shai, Y. (1999) *Biochim. Biophys. Acta* **1462,** 55–70.
14. Wu, M., Maier, E., Benz, R. & Hancock, R. E. (1999) *Biochemistry* **38,** 7235–7242.
15. Mor, A. & Nicolas, P. (1994) *J. Biol. Chem.* **269,** 1934–1939.
16. Matsuzaki, K., Murase, O., Fujii, N. & Miyajima, K. (1996) *Biochemistry* **35,** 11361–11368.
17. Ludtke, S. J., He, K., Heller, W. T., Harroun, T. A., Yang, L. & Huang, H. W. (1996) *Biochemistry* **35,** 13723–13728.
18. Lohner, K. (2001) *Development of Novel Antimicrobial Agents: Emerging Strategies* (Horizon Scientific Press, Wymondham, U.K.).
19. Epand, R. M. & Vogel, H. J. (1999) *Biochim. Biophys. Acta* **1462,** 11–28.
20. Graham, J. M. (1997) *Membrane Analysis* (Springer, New York).
21. Ratledge, C. & Wilkinson, S. G. (1988) *Microbial Lipids* (Academic, London).
22. Kokryakov, V. N., Harwig, S. S., Panyutich, E. A., Shevchenko, A. A., Aleshina, G. M., Shamova, O. V., Korneva, H. A. & Lehrer, R. I. (1993) *FEBS Lett.* **327,** 231–236.
23. Ganz, T. & Lehrer, R. I. (1995) *Pharmacol. Ther.* **66,** 191–205.
24. Tang, Y. Q., Yuan, J., Miller, C. J. & Selsted, M. E. (1999) *Infect. Immun.* **67,** 6139–6144.
25. Aumelas, A., Mangoni, M., Roumestand, C., Chiche, L., Despaux, E., Grassy, G., Calas, B. & Chavanieu, A. (1996) *Eur. J. Biochem.* **237,** 575–583.
26. Fahrner, R. L., Dieckmann, T., Harwig, S. S., Lehrer, R. I., Eisenberg, D. & Feigon, J. (1996) *Chem. Biol.* **3,** 543–550.
27. Harwig, S. S., Waring, A., Yang, H. J., Cho, Y., Tan, L. & Lehrer, R. I. (1996) *Eur. J. Biochem.* **240,** 352–357.
28. Qu, X. D., Harwig, S. S., Oren, A. M., Shafer, W. M. & Lehrer, R. I. (1996) *Infect. Immun.* **64,** 1240–1245.
29. Qu, X. D., Harwig, S. S., Shafer, W. M. & Lehrer, R. I. (1997) *Infect. Immun.* **65,** 636–639.
30. Cho, Y., Turner, J. S., Dinh, N. N. & Lehrer, R. I. (1998) *Infect. Immun.* **66,** 2486–2493.
31. Tamamura, H., Murakami, T., Horiuchi, S., Sugihara, K., Otaka, A., Takada, W., Ibuka, T., Waki, M., Yamamoto, N. & Fujii, N. (1995) *Chem. Pharm. Bull.* **43,** 853–858.
32. Sokolov, Y., Mirzabekov, T., Martin, D. W., Lehrer, R. I. & Kagan, B. L. (1999) *Biochim. Biophys. Acta* **1420,** 23–29.
33. Bellm, L., Lehrer, R. I. & Ganz, T. (2000) *Expert Opin. Invest. Drugs* **9,** 1731–1742.
34. Nouri-Sorkhabi, M. H., Wright, L. C., Sullivan, D. R. & Kuchel, P. W. (1996) *Lipids* **31,** 765–770.
35. Nouri-Sorkhabi, M. H., Agar, N. S., Sullivan, D. R., Gallagher, C. & Kuchel, P. W. (1996) *Comp. Biochem. Physiol. B Biochem. Mol. Biol.* **113,** 221–227.
36. Schlossman, M. L., Synal, D., Guan, Y. M., Meron, M., Shea-McCarthy, G., Huang, Z. Q., Acero, A., Williams, S. M., Rice, S. A. & Viccaro, P. J. (1997) *Rev. Sci. Instrum.* **68,** 4372–4384.
37. Konovalov, O., Myagkov, I., Struth, B. & Lohner, K. (2002) *Eur. Biophys. J.* **31,** 428–437.
38. Als-Nielsen, J., Jacquemain, D., Kjaer, K., Leveiller, F., Lahav, M. & Leiserowitz, L. (1994) *Phys. Rep.* **246,** 251–313.